Modulation of Aldose Reductase Inhibition by Halogen Bond Tuning

ARTICLE *in* ACS CHEMICAL BIOLOGY · AUGUST 2013

Impact Factor: 5.33 · DOI: 10.1021/cb400526n · Source: PubMed

14 AUTHORS, INCLUDING:

Francesc Xavier Ruiz
Rutgers, The State University of New Jersey
27 PUBLICATIONS **361** CITATIONS
SEE PROFILE

Martin Lepsík
Academy of Sciences of the Czech Republic
53 PUBLICATIONS **697** CITATIONS
SEE PROFILE

Alberto Podjarny
Institut de Génétique et de Biologie Molécul…
66 PUBLICATIONS **891** CITATIONS
SEE PROFILE

Pavel Hobza
Academy of Sciences of the Czech Republic
320 PUBLICATIONS **18,189** CITATIONS
SEE PROFILE

ACS chemical biology

Articles

pubs.acs.org/acschemicalbiology

Modulation of Aldose Reductase Inhibition by Halogen Bond Tuning

Jindřich Fanfrlík,*[,†] Michal Kolář,[†] Martin Kamlar,[‡] David Hurný,[‡] Francesc X. Ruiz,[§] Alexandra Cousido-Siah,[§] André Mitschler,[§] Jan Řezáč,[†] Elango Munusamy,[∥] Martin Lepšík,[†] Pavel Matějíček,[⊥] Jan Veselý,[‡] Alberto Podjarny,*[,§] and Pavel Hobza[†,#]

[†]Institute of Organic Chemistry and Biochemistry and Gilead Science Research Center, Academy of Sciences of the Czech Republic, Flemingovo nam. 2, 166 10 Prague 6, Czech Republic

[‡]Department of Organic Chemistry, Charles University in Prague, Hlavova 2030, 128 43 Prague 2, Czech Republic

[§]Department of Integrative Biology, IGBMC, CNRS, INSERM, UdS, 1 rue Laurent Fries, 67404 Illkirch CEDEX, France

[∥]Department of Chemistry, Texas A&M University, College Station, Texas 77842, United States

[⊥]Department of Physical and Macromolecular Chemistry, Charles University in Prague, Hlavova 2030, 128 43 Prague 2, Czech Republic

[#]Regional Centre of Advanced Technologies and Materials, Department of Physical Chemistry, Palacký University, Olomouc, 771 46 Olomouc, Czech Republic

Supporting Information

ABSTRACT: In this paper, we studied a designed series of aldose reductase (AR) inhibitors. The series was derived from a known AR binder, which had previously been shown to form a halogen bond between its bromine atom and the oxygen atom of the Thr-113 side chain of AR. In the series, the strength of the halogen bond was modulated by two factors, namely bromine−iodine substitution and the fluorination of the aromatic ring in several positions. The role of the single halogen bond in AR−ligand binding was elucidated by advanced binding free energy calculations involving the semiempirical quantum chemical Hamiltonian. The results were complemented with ultrahigh-resolution X-ray crystallography and IC_{50} measurements. All of the AR inhibitors studied were shown by X-ray crystallography to bind in an identical manner. Further, it was demonstrated that it was possible to decrease the IC_{50} value by about 1 order of magnitude by tuning the strength of the halogen bond by a monoatomic substitution. The calculations revealed that the protein−ligand interaction energy increased upon the substitution of iodine for bromine or upon the addition of electron-withdrawing fluorine atoms to the ring. However, the effect on the binding affinity was found to be more complex due to the change of the solvation/desolvation properties within the ligand series. The study shows that it is possible to modulate the strength of a halogen bond in a protein−ligand complex as was designed based on the previous studies of low-molecular-weight complexes.

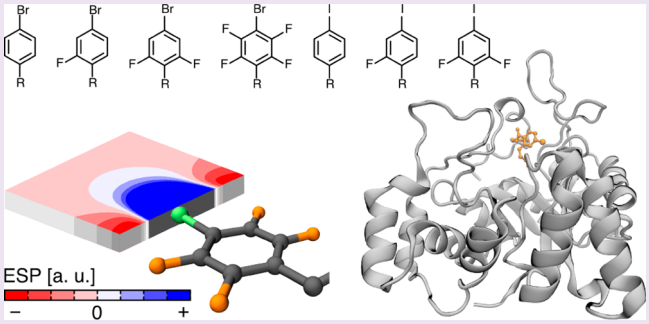

A halogen bond (X-bond) is a noncovalent interaction that can be utilized in medicinal chemistry[1−3] and crystal engineering.[4,5] Various X-bond types were found to be important in many pharmaceutically relevant protein−ligand (P−L) complexes.[6−12] In biomolecular complexes, halogen bonds occur between heavier halogens (I, Br, Cl) and electronegative elements (or electron donors) such as oxygen and nitrogen[2,13−15] or electron-rich moieties such as the phenyl ring.[16] The binding is facilitated by the electrostatic interaction between the σ-hole (a region with a positive electrostatic potential)[17,18] located at the top of the halogen atoms (along the C-X bond axis) and negatively charged electronegative atoms. However, quantum chemical calculations showed that the dispersion interaction was also a non-negligible factor.[19] The size of the σ-hole, which determines the strength of the halogen bond, can be modulated by two factors: (i) the chemical environment of the halogen and (ii) the nature of the halogen.[20,21] For example, the chemical environment can be modified by fluorine substitution on the aromatic ring near the halogen involved in the X-bond. It can have a dramatic effect; the gas-phase binding energy of pentafluorochlorobenzene-acetone was calculated to be 102% higher than that of the chlorobenzene-acetone complex.[20] Further, the X-bond strength depends on the nature of the halogen in such a way that the higher the atomic number of the halogen, the stronger the X-bond formed.[20] Apart from small molecular complexes, this has already been confirmed also in P−L complexes. Chlorine replacement by bromine and iodine enhanced the

Received: July 12, 2013
Accepted: August 30, 2013

   dx.doi.org/10.1021/cb400526n | ACS Chem. Biol. XXXX, XXX, XXX−XXX

interactions in the cathepsin−inhibitor complex and reduced IC_{50} from 30 nM to 6.5 and 4.3 nM, respectively.[22]

To study halogen bonding in a protein−ligand complex, we have chosen the human aldose reductase (AR). It catalyzes the NADPH-dependent conversion of glucose to sorbitol, the first step in the polyol pathway of glucose metabolism.[23] Under standard glycemic conditions, the polyol pathway is not important. However, in response to hyperglycemic conditions (e.g., diabetes), this pathway might represent up to 33% of the total glucose turnover.[24] AR has been established as a promising therapeutic target for the treatment of diabetic complications.[24] Moreover, AR has recently been related to a number of inflammatory diseases such as atherosclerosis, sepsis, asthma, allergic rhinitis, and uveitis.[25,26] Also, AR has been shown to be involved in cancer, especially colon carcinoma and hepatocellular carcinoma,[27,28] and AR inhibition has been reported to prevent colon cancer metastasis.[29]

Attention has thus been paid to the binding process of the inhibitors to AR. Many AR inhibitors (ARIs) have been synthesized and ultrahigh-resolution X-ray structures (up to 0.66 Å) have been solved.[29−36] IDD388 is an ARI that contains a bromine atom participating in an X-bond with an oxygen atom of the side chain of Thr-113 of AR.[37] This makes the AR:$NADP^+$:IDD388 complex a suitable model case for X-bond tuning. The structure and strength of the AR-IDD388 halogen bond has already been studied by X-ray analysis and isothermal titration calorimetry against a mutation series of single-site mutants of the wild-type AR. It was shown that the mutation of Thr-113 to Ala-113 caused the loss of the binding free energy of IDD388 to AR by about 1.3 kcal mol^{-1}.[35] Here, we study the effect of the ligand modification on the strength of the X-bond. Based on IDD388 and its iodine analogue, we designed a series of mono-, di-, and tetra-fluorinated compounds to study systematically the effect of fluorine substitutions on the strength of the X-bond in P−L complexes.

To estimate the binding free energy computationally, we employed an advanced scoring function based on using the multilayer QM/SQM/MM hybrid approach. Specifically, we used DFT-D[38] for quantum mechanics (QM), PM6-D3H4X[39−42] for semiempirical QM (SQM), and AMBER[43,44] for molecular mechanics. The methods based on DFT and PM6 include empirical corrections for dispersion interaction (D), hydrogen- (H), and halogen- (X) bonding to obtain a quantitative description of noncovalent interactions.[38−42] The resulting methods were shown to describe faithfully dispersion interactions, the directionality, and the strength of H- and X-bonds and to provide interaction energies comparable with high-level *ab initio* benchmark data.[41] The scoring function approximates the P−L binding affinity by a sum of energetic terms and includes gas-phase interaction energy, a change of solvation free energy and a change of conformational 'free' energy.[45,46] The composition of the scoring function is modular. An important feature of our scoring function is that the terms describe physically meaningful phenomena that occur upon binding. Previously, the scoring function based on SQM and QM/SQM/MM was successfully applied to three types of P−L complexes, namely the HIV-1 protease,[45] cyclin-dependent kinase 2,[47,48] and casein kinase 2,[49] binding to a series of inhibitors. It is thus a well-established tool of computational biochemistry.[46]

In this study, the scoring function based on DFT-D/PM6-D3H4X/MM methodology was used to predict and explain the effect of ligand modification on the strength of the X-bond and inhibition activity. To validate the computational data, the designed inhibitors were synthesized and their IC_{50} values (i.e., binding affinities) to recombinant AR were measured. Furthermore, the experimental X-ray structures were determined at ultrahigh resolution.

2. RESULTS AND DISCUSSION

2.1. Synthesis and Binding Affinities. Based on our knowledge of the X-bond obtained on small model complexes, we designed, modeled, and scored a series of IDD388-like inhibitors. To validate the approach and calculations, we synthesized the compounds and measured their affinities toward AR (Table 1 and Figure 1).

Table 1. Structural Formula of the Studied Inhibitors and Experimental IC_{50} in μM

	substituent position					
inhibitor	X	2	3	5	6	IC_{50}
			Bromine Series			
MK181	Br	H	H	H	H	0.71 ± 0.07
IDD388	Br	F	H	H	H	0.40 ± 0.02
MK408	Br	F	H	H	F	1.19 ± 0.09
MK319	Br	F	F	F	F	0.30 ± 0.02
			Iodine Series			
MK257	I	H	H	H	H	1.90 ± 0.10
MK315	I	F	H	H	H	0.19 ± 0.09
MK409	I	F	H	H	F	1.36 ± 0.06

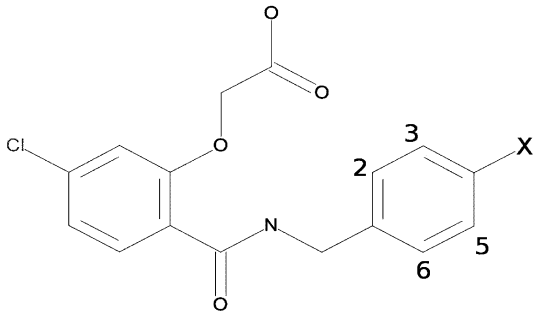

Figure 1. Structural formula of the AR inhibitors.

IC_{50} values ranged from 0.2 μM to 1.9 μM. Considering that the tightest binding and the least binding compounds (MK257 and MK315) differ only in one atom (H vs F), the change of 1 order of magnitude is quite substantial. The IC_{50} values of unsubstituted and difluorinated bromine ARIs were higher (0.7 and 1.2 μM for MK181 and MK408, respectively) than those of mono- and tetra-fluorine substituted bromine-containing ARIs (a IC_{50} of 0.4 and 0.3 μM for IDD388 and MK319, respectively). Similarly, unsubstituted and difluorinated iodine ARIs had a higher IC_{50} than the monofluorinated iodine inhibitor (an IC_{50} of 1.9, 1.4, and 0.3 μM, for MK257, MK409, and MK315, respectively). It must be noted that such variations cannot be related to the structure of AR complexes, because they are structurally quite invariable (see later). Here, the computational models might provide valuable insight.

IC_{50} is the parameter checked in pharmaceutical screens for AR, and its inhibitors usually exhibit uncompetitive inhibition.[50,51] Moreover, in this work, they have been compared under the same experimental conditions, which means that IC_{50}

dx.doi.org/10.1021/cb400526n | ACS Chem. Biol. XXXX, XXX, XXX−XXX

is a relative parameter that allows us to compare the binding affinity of the inhibitors.

2.2. X-ray Structures of AR Inhibitor Complexes. For building *in-silico* models of the complexes (see Section 2.3.), the ternary complex of AR:NADP$^+$:IDD388 (PDB code 2IKI)[33] was used as the starting point. Such a computational approach decreases the variability of the models and thus provides a better focus on the problem (i.e., fluorination and X-bond-involving halogen substitution).[46]

Even though the ligands are similar, the assumption to build the models of the complexes by modifying the 2IKI complex needs to be justified. The bromine−iodine and hydrogen−fluorine pairs of atoms differ in their van der Waals radii by about 10%. In the AR complex, the distance between the bromine atom of the inhibitor and the oxygen atom of Thr-113 of the AR in the 2IKI complex is shorter than the sum of van der Waals radii (2.90 Å).

To validate the computational models, all of the complex structures were determined at ultrahigh resolution (<1 Å; for details, see the Supporting Information). With such resolution, the level of the details observed in the best-ordered areas approaches that of small-molecule studies. In fact, atoms and bond densities are clearly visible, which makes the estimation of the atomic charges possible.[37] To demonstrate this, the omit difference map of compound MK319 is shown and all the atoms of the inhibitor are clearly observed (Figure 2). The AR

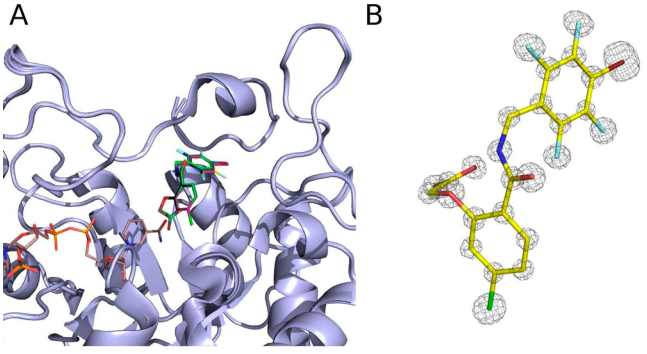

Figure 2. X-ray crystallography determination of the AR:NADP$^+$:inhibitor complexes. (A) An overview of all the structures represented in cartoon (gray) and the AR inhibitor and cofactor (brown) in sticks; (B) an MK319 omit difference map displaying the inhibitor electron density (gray) calculated with a 10σ cutoff, with the inhibitor in sticks.

inhibitor-binding sites and the AR-inhibitor positioning were nearly equivalent in all the cases, and the addition of a fluorine atom did not provide any new significant interactions that could explain the differences in the binding affinity detected by the IC_{50} measures (Figure 3).

2.3. Computational Modeling. The modeled complexes were optimized and the binding free energy was approximated by the total score expressed by eq 1 (ref 45)—a new consistent notation is in ref 46 and 48.

$$\text{Score} = \Delta E_{\text{int}} + \Delta\Delta G_{\text{solv}} + \Delta G'^{\text{w}}_{\text{conf}}(\text{L}) \quad (1)$$

$$\Delta\Delta G_{\text{solv}} = \Delta\Delta G_{\text{int,solv}} + (\Delta G^{\text{low}}{}_{\text{solv}}(L) - \Delta G^{\text{high}}{}_{\text{solv}}(L)) \quad (2)$$

Particular terms describe the gas-phase interaction energy (ΔE_{int}), the interaction solvation/desolvation free energy ($\Delta\Delta G_{\text{solv}}$), and the change of the conformational 'free' energy

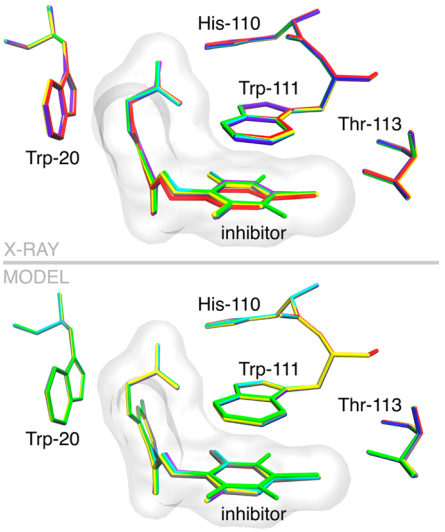

Figure 3. Alignment of the AR inhibitors and selected amino acids of the AR active site based on experimental structures (X-ray, upper panel) and QM/SQM/MM optimized structures (Model, lower panel). The coloring is as follows: MK181 in blue, IDD388 in violet, MK408 in cyan, MK319 in green, MK257 in red, MK315 in gray, and MK409 in yellow.

of ligand ($\Delta G'^{\text{w}}_{\text{conf}}(L)$). The ΔE_{int} was calculated using the QM/SQM/MM method (see Methods). The solvation free-energy change $\Delta\Delta G_{\text{int,solv}}$ is determined by the generalized Born (GB) solvent model implemented in AMBER10.[52] In our score, SMD/HF/6-31G*[53,54] is also used, because this method describes the solvation free energy more accurately for drug molecules.[55] However, the SMD method is so computationally demanding that it is used only for the ligand, giving rise to the correction of ligand solvation/desolvation ($\Delta G^{\text{low}}{}_{\text{solv}}(L) - \Delta G^{\text{high}}{}_{\text{solv}}(L)$), which is the difference between the solvation free energy calculated at high (SMD) and low (GB) levels of theory. The use of SMD scheme for solvation energy changes is especially important for a correct description of charged inhibitors.[45] The $\Delta G'^{\text{w}}_{\text{conf}}(L)$ term is the 'free' energy change between the ligand in its optimal solution structure and the ligand conformation adopted in the P−L complex. For the evaluation of $\Delta G'^{\text{w}}_{\text{conf}}(L)$, the gas phase DFT-D (TPSS/TZVP//B-LYP/SVP) energy is combined with the SMD solvation free energy. A detailed description of all the terms can be found in refs 45 and 46.

2.3.1. Gradient Optimization of AR−Inhibitor Complexes. All the modeled complexes were optimized by using advanced QM/SQM/MM methodology. The X-bond lengths and angles of optimized complexes are summarized in Supporting Information Table S2 (see also Figure 4). Structures obtained by the QM/SQM/MM optimization are very close to the X-ray

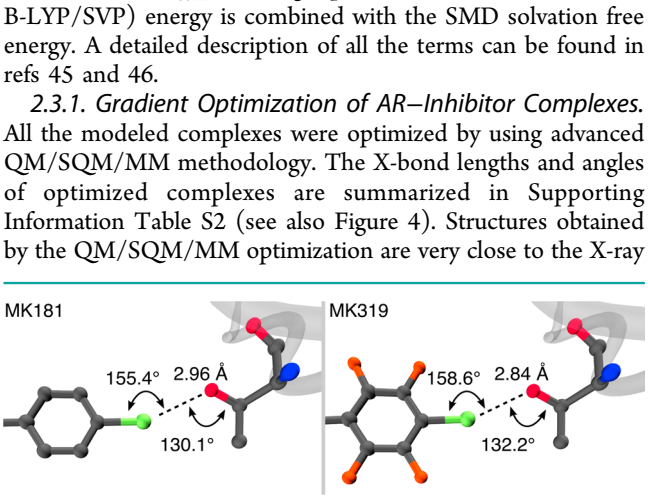

Figure 4. Geometries of halogen bond between Thr-113 and unsubstituted bromophenyl (left) and tetrafluorinated bromophenyl (right) ligands determined by X-ray crystallography.

dx.doi.org/10.1021/cb400526n | ACS Chem. Biol. XXXX, XXX, XXX−XXX

structures (Supporting Information Table S2 and Figure 3). A maximum difference in X-bond length between X-ray and QM/SQM/MM structures is only 0.11 Å (in the complex of MK257). Similarly, maximum differences for the C−X···O and X···O−C angles are 6.33° and 4.72°, respectively (complexes of MK319 and MK315, respectively). The QM/SQM/MM structures also enable us to compare orientation of hydrogen atoms. They show that orientation of the hydrogen of the hydroxyl group in Thr-113 is conserved within the AR−inhibitor complexes. The hydrogen forms a hydrogen bond with the carbonyl group of the peptide bond between Thr-113 and Gly-114.

Additionally, the AR−inhibitor complexes were reoptimized by the standard AMBER potential combined with GB solvent model for comparison. Structures of AR−inhibitor complex obtained using AMBER optimization differ considerably more. The X-bond is broken upon the AMBER optimization. The X···O distance increases by about 0.5 Å and thus becomes larger than the sum of van der Waals radii. Moreover, the C−X···O angle becomes more bent by about 10° to 20°. This is a known drawback of molecular-mechanical description of X-bond.[56]

2.3.2. Gas-Phase Interaction Energy (ΔE_{int}). Br···O X-bond Series. The first column of Table 2 shows the calculated gas-phase interaction energies for P−L complexes determined by optimization in water environment (ΔE_{int}). The MK181 (no fluorine atoms) inhibitor is taken as the reference to which the ΔE_{int} of IDD388 (one fluorine), MK408 (two fluorine atoms), and MK319 (four fluorine atoms) compounds are compared. Withdrawing the electrons from the phenyl ring by the fluorine atoms results in a larger region with a more positive electrostatic potential (ESP) on the bromine (see Figure 5). This effect may be considered to increase the size and deepen the σ-hole. Obviously, the fluorine substitution makes the gas-phase interaction energy more negative (i.e., favoring the complex formation). We claim that such an energy change is directly related to the size and depth of the σ-hole. The mono-, di-, and tetra-fluorine substitutions made ΔE_{int} more negative by 0.8, 2.2, and 3.2 kcal mol^{-1}, respectively.

Table 2. Calculated Gas-Phase Interaction Energy (ΔE_{int}), Interaction Desolvation Free Energy ($\Delta\Delta G_{solv}$), Scores, and Experimental $\Delta G_b°$ (Calculated by $\Delta G_b° = RT \ln(IC_{50}/2)$)[a] in kcal mol^{-1}

inhibitor	ΔE_{int}	$\Delta\Delta G_{solv}$	score	$\Delta G_b°$
		Bromine Series		
MK181	−81.2	35.8	−45.4	−8.8
IDD388	−82.0	34.4	−47.6	−9.1
MK408	−83.4	37.2	−46.3	−8.5
MK319	−84.3	35.1	−49.1	−9.3
		Iodine Series		
MK257	−84.0	38.3	−45.2	−8.2
MK315	−85.8	37.8	−48.0	−9.6
MK409	−86.9	39.8	−47.1	−8.4

[a] $\Delta G_b°$ refers to free energy for the reaction under standard conditions of all reactants and products at a concentration of 1.0 M

I···O X-bond Series. Similar trends have been observed for iodinated series as well. The size and the depth of the σ-hole increases with the number of fluorine atoms (Figure 5), which corresponds to more negative ΔE_{int}. Tetra-fluorine substitution was not considered due to the low stability of the compound. When compared to MK257, the ΔE_{int} of MK315 and MK409 become more negative by 1.8 and 2.8 kcal mol^{-1}, respectively, which favors binding.

Focusing on bromine−iodine exchange, the trends known from small molecular complexes are observed also here. The iodinated compounds bind more strongly than the brominated ones, in accordance with the sizes of the σ-holes and larger polarizability. The changes are 2.8, 3.8, and 3.4 kcal mol^{-1} for unsubstituted, monosubstituted, and disubstituted inhibitors, respectively.

The gas-phase interaction energies alone do not correlate with the experimental binding data (a coefficient of determination (R^2) of 0.01 and a predictive index (PI) of 0.09). This hints that other energetic terms come into play.

2.3.3. Changes in Solvation Free Energy upon Complex Formation ($\Delta\Delta G_{solv}$). The second column in Table 2 summarizes the calculated changes in solvation free energy upon complex formation ($\Delta\Delta G_{solv}$). The $\Delta\Delta G_{solv}$ of MK181 (bromo-) and MK319 (iodo-) inhibitors were taken as the reference to which $\Delta\Delta G_{solv}$ of fluorine-substituted compounds were compared. Monofluorine substitution decreased $\Delta\Delta G_{solv}$ by 1.4 kcal mol^{-1} for Br-containing inhibitors. The same trend was found also for iodinated inhibitors, but the difference was

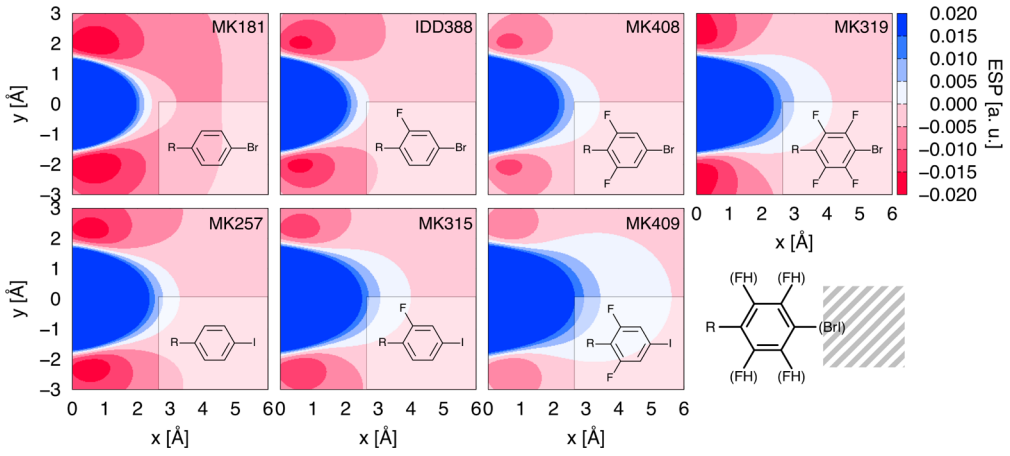

Figure 5. Electrostatic potential (ESP) maps calculated for the region, which is hatched in the bottom right-hand corner. The halogen involved in the X-bond (bromine or iodine) lies at the origin of the coordinate system.

dx.doi.org/10.1021/cb400526n | ACS Chem. Biol. XXXX, XXX, XXX−XXX

smaller (a change in the $\Delta\Delta G_{solv}$ of about 0.5 kcal mol^{-1}). In contrast to monofluorine substitution, the difluorine substitution increased the $\Delta\Delta G_{solv}$ by about 1.5 kcal mol^{-1} in both the bromine and iodine cases. The tetra-fluorine substitution slightly decreased the $\Delta\Delta G_{solv}$ (by about 0.7 kcal mol^{-1}).

Since the structures of active sites are well-conserved, it is valid to expect that the solvation variations lie in the solvation free energy variations of the ligand only. In order to understand the solvation features, the isolated ligands were computationally studied by two distinct models: SMD[53] and COSMO-RS/BP86/TZVP.[57] It was found, in accordance with the $\Delta\Delta G_{solv}$ term of the score, that disubstituted ligands are better hydrated, thus the penalty for moving them to the hydrophobic environment of the protein is higher when compared to the other substitutions.

A comparison of brominated and iodinated inhibitors showed that the bromine−iodine exchange systematically increases the value of $\Delta\Delta G_{solv.}$ For the iodine analogues, $\Delta\Delta G_{solv}$ is more positive by about 2.5, 3.4, and 2.6 kcal mol^{-1} for unsubstituted, monofluorinated and difluorinated inhibitors, respectively.

2.3.4. Score. The total score is shown in the third column of Table 2, and it is plotted against experimental binding free energies in Figure 6. The score reasonably correlates with the

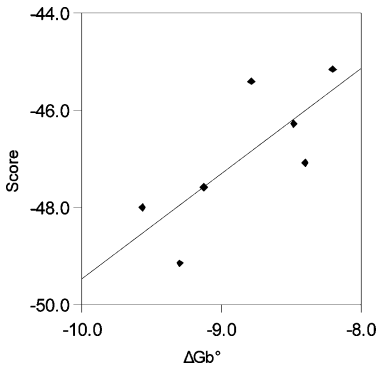

Figure 6. Total score plotted against experimental ΔG_b° (in kcal mol^{-1}). The coefficient of determination (R^2) is 0.59 and the predictive index (PI) is 0.83.

experiment (a R^2 of 0.59 and a PI of 0.83). It was constructed as a sum of ΔE_{int}, $\Delta\Delta G_{solv}$, and $\Delta G'^{w}_{conf}(L)$.[45,46] The change in protein (P) conformational free energy was expected to be identical within the ligand series. Unlike in our previous studies, the problem of entropy change was not treated by vibrational analysis at the MM level due to the problematic description of this term for halogen-bond complexes at the MM level.[49] It should be, however, mentioned here that some portion of the entropy contribution is included in $\Delta\Delta G_{solv}$ via the parametrization of the implicit solvent model.[53] An error cancellation cannot also be ruled out. The ligands as well as the P−L active sites are similar and thus the differences in their conformational behavior will probably be so similar that their neglect will not alter the results substantially.

Contrary to the ΔE_{int} and $\Delta\Delta G_{solv}$ terms, the conformational 'free' energy ($\Delta G'^{w}_{conf}(L)$) did not play an important role in this study. MK257 was the only inhibitor for which the value was not negligible (of 0.6 kcal mol^{-1}; $\Delta G'^{w}_{conf}(L)$ not shown in Table 1). This could be caused by the larger radius of the iodine atom (as compared to the bromine atom) and a smaller σ-hole in comparison with the fluorine-substituted compounds. The score thus reflects mainly the balance between ΔE_{int} and $\Delta\Delta G_{solv}$. The negative sign of ΔE_{int} states that this terms favors complex formation. We speculate that it is thanks to the increased strength of the halogen bond caused by the fluorination. On the other hand, $\Delta\Delta G_{solv}$ goes against binding (it has positive values). While the mono- and tetra-fluorine substitutions decreased $\Delta\Delta G_{solv}$ and hence supported binding, difluorine substitutions had the opposite effect and supported complex dissociation. Consequently, the scores of mono- and tetra-fluorinated compounds were calculated to be more negative (ranging from −47.6 to −49.1 kcal mol^{-1}) than those of nonsubstituted and difluorine substituted compounds (with the score ranging from −45.2 to −47.1 kcal mol^{-1}). It should be also mentioned that the use of SMD scheme for the ligand solvation/desolvation is especially important in this study for the description of the electrostatic anisotropy of the heavier halogens (that is, the σ-hole of bromine and iodine). When the SMD scheme is not used the correlation between of the calculated score with experiment becomes insignificant (R^2 of 0.05 and PI of 0.14).

In order to unanimously describe the trends and effects of the X-bond, the standard AMBER score was also calculated (Supporting Information Table S3). The AMBER score is applied to the AMBER optimized structures and the solvation free energy change is consistently determined by the GB solvent model here. The SMD scheme for ligand solvation energy changes is not used in the AMBER score. The AMBER score does not correlate with the experimental data (R^2 of 0.14 and PI of 0.24; see Supporting Information Graph S1). It is not surprising since standard MM methods do not describe the electrostatic anisotropy of halogen atoms. MM methods can, however, be modified in an elegant way by introduction of a dummy atom having a positive partial charge (explicit σ-hole, ESH) close to a halogen atom.[56] A scoring function based on AMBER with the explicit σ-hole is being developed.[58]

2.4. Conclusions. We have shown that it is possible to tune the strength of halogen bonding in a P−L complex and decrease IC_{50} by about 1 order of magnitude by a monoatomic substitution. The structural changes in the ternary complexes were shown by ultrahigh-resolution X-ray crystallography to be minimal upon ligand modifications. By means of computational techniques, the fluorine substitutions and bromine−iodine interchange systematically increase the gas-phase interaction energy. This correlates with the increasing size of the σ-hole, which is in agreement with previous studies.[20] The increase of binding affinity, expressed in terms of IC_{50}, is, however, not systematic. This can be explained by the role of solvation/desolvation contributions. It was calculated that the two-fluorine substitution (MK408 and MK409) increases the desolvation penalty, making the total score least favorable as compared to the other analogues. The delicate balance between the σ-hole size and solvation/desolvation changes for the resulting strength of the binding affinity of the AR inhibitors emphasized the need to combine both the experimental and computational data to improve the drug-design success.

3. METHODS

3.1. Molecular Modeling and Calculations. The P−L complexes were modeled from the X-ray structure taken from the Protein Data Bank (PDB code: 2IKI).[33] Arg, Lys, Asp, Glu, ligands (charge −1 due to the COO^- group), $NADP^+$ (charge of −3), and N- and C-termini were considered as ionic. All

dx.doi.org/10.1021/cb400526n | ACS Chem. Biol. XXXX, XXX, XXX−XXX

other residues were considered as neutral. All of the crystal-water molecules were removed.

To treat such large systems effectively, we used a subtractive QM/MM scheme.[59] Specifically, we employed the triple(QM/SQM/MM)-layer variant. The substructive scheme couples the small QM region treated by the DFT-D (TPSS/TZVP//B-LYP/SVP)[38] level of theory and the large SQM region treated by PM6-D3H4X[39−42] with an MM description for the rest of the system. The QM/MM procedure is implemented in a Cuby[60] framework developed in our laboratory. It calls Turbomole6.3[61] for the QM calculation, MOPAC2009[62] for the SQM calculation and AMBER10[43,44] for the MM calculations. The SQM part comprised the inhibitor, the $NADP^+$ cofactor, and the amino acids that were within 8 and 4 Å from the studied inhibitor and $NADP^+$, respectively. The resulting SQM part contained about 1370 atoms. The QM part comprised the inhibitor and residues 112−115 (i.e., it contained the T113). The rest of the AR complex was treated by MM. For the protein, the parm03 force field[43] from the AMBER family of force fields was used. The MM parameters for $NADP^+$ were adopted from previous studies.[63−65] The atoms of all of the ligands were described by the General AMBER Force Field (GAFF),[43] which covers a wide range of organic molecules and is compatible with other AMBER force fields. The partial charges on the ligand atoms were assigned according to the Restrained Electrostatic Potential (RESP) procedure[44] calculated on the HF/6-31G* level[44] (the DGDZVP basis set was used for iodine atoms) to remain consistent with the description of the protein and cofactor. The inhibitor charges were fitted to represent a grid of ESP points calculated around DFT-D optimized structure using Gaussian09.[54] For comparison of halogen σ-holes, the ESP was calculated in the plane of particular aromatic ring at higher level of theory, namely at the B3LYP/def-TZVPP level employing pseudopotentials for iodine in order to include the relativistic effects. The maps were calculated for isolated neutral inhibitors using the same geometries as used for RESP.

The structures of all the P−L complexes were systematically optimized by using FIRE algorithm[66] with the following optimization criteria: energy change < 0.006 kcal mol^{-1}, the largest gradient component < 1.2 kcal mol^{-1} $Å^{-1}$, and the root-mean-square gradient < 0.6 kcal mol^{-1} $Å^{-1}$.

We used the coefficient of determination (R^2) and also the predictive index (PI) to analyze the correlation between the calculated and experimental data. The PI is a measure of the reliability of a prediction method in the context of normal use.[67] The PI judges the ranking; if it is equal to +1.0, it stands for perfect correct prediction, −1.0 for perfect incorrect prediction, and 0.0 for random. The definition of the PI includes a weighing term. The weighing term depends on the difference between the experimental values to reflect the changes that result in large differences in the binding. Similarly, the changes that cause only little differences in the binding have a small impact on the PI.

3.2. Experimental Procedures. *3.2.1. IC_{50} Studies.* The IC_{50}-activity assays were carried out based on the quantification of the NADPH consumption that takes place when the enzyme catalyzes the conversion of glyceraldehyde into glycerol. The assays were performed at 25 °C in a 100 mM sodium phosphate buffer (pH 7.0), with the AR protein amount reaching the V_{max}, and 0.2 mM NADPH. The final reaction volume was 500 μL per reaction. All compounds were dissolved in dimethyl sulphoxide, and the corresponding solution was added to the cell and incubated for 5 min at 25 °C prior to the addition of the substrate. The reaction was initiated by the addition of 1 mM glyceraldehyde, and the decrease in optical density at 340 nm was monitored for 3 min at 25 °C in a UV−vis spectrophotometer (UV-1700 PharmaSpec, Shimadzu). The IC_{50} value was determined as the compound concentration that inhibits the enzymatic activity by 50%. IC_{50} was calculated using the Grafit program (version 5.0; Erithacus Software) and the values were determined as the mean of three experiments ± the standard deviation.

3.2.2. Crystallization, Structure Determination, and Refinement. The crystals of AR:$NADP^+$:ARI were obtained by cocrystallization under the published conditions[30] (50 mM ammonium citrate, pH 5.0, 20% polyethylene glycol, PEG 6000) by the hanging-drop vapor-diffusion method at 24 °C. Cryo-cooling in liquid nitrogen was carried out using a cryo-protecting solution containing 40% PEG 6000. The data collection was performed on the synchrotron X06SA beamline at the Swiss Light Source. The crystals belong to the $P2_1$ space group, with one protein molecule in the asymmetric unit. The atomic coordinates of the human AR:$NADP^+$:IDD594 complex (PDB code 1US0), which is the highest-resolution AR structure available, were used to solve the structure of the AR ternary complex. Crystallographic refinement involved repeated cycles of conjugate gradient energy minimization and temperature factor refinement, performed with the CCP4 suite.[68] Amino-acid side chains were fitted into $2F_o-F_c$ and F_o-F_c electron-density maps. The final F_o-F_c map indicated clear electron density for the different inhibitors. The Phenix[69] and Coot[70] programs were used for fitting the models into the electron density. The data collection and the refinement statistics are listed in the Supporting Information. The atomic coordinates have been deposited in the PDB (ID codes: 4LAU, 4LAZ, 4LB3, 3LB4, 4LBR, 4LBS) and will be released immediately upon publication.

3.2.3. Organic Synthesis. A synthesis of the designed series of ARIs was carried out based on the reported procedure[28] via the base-promoted amide formation from halogenated benzylamine hydrochlorides and *in situ* prepared salicyl chloride, followed by *O*-alkylation with ethyl bromoacetate and the subsequent hydrolysis of ethyl ester moiety. The corresponding benzylamine hydrochlorides were prepared either from halogenated toluenes via radical bromination followed by azidation and the subsequent Staudinger reduction, or from halogenated benzoic acid via amidation and reduction.

Such physicochemical characteristics as the absorption spectra and the tendency to aggregate were determined for the compounds in aqueous and *n*-octanol solutions. The typical band for all the compounds is observed at 291 nm. All the solutions are clear and stable with no tendency to form a significant fraction of multimolecular aggregates.

The full characterization (^1H, ^{19}F, and ^{13}C NMR, IR, HRMS) of all the AR inhibitors and their key intermediates along with detailed working procedures for their preparation are listed in the Supporting Information. All the chemicals and solvents used in this part were either purchased (puriss p.a.) from commercial suppliers or purified by standard techniques. The reactions were monitored by thin-layer chromatography (TLC, silica-gel plates Merck 60 F254).

The flash chromatography purification of ARIs was performed by using silica gel Merck 60 (a particle size 0.040−0.063 mm). The ^1H, ^{19}F and ^{13}C NMR spectra were recorded with Bruker AVANCE III 600 or Varian VNMRs 300

instruments. The high-resolution mass spectra were recorded with a LTQ Orbitrap XL spectrometer. The IR DRIFT spectra were recorded with Nicolet AVATAR 370 FT-IR in cm^{-1}.

■ ASSOCIATED CONTENT

Supporting Information

The atomic coordinates deposited in the PDB (the ID codes), the data collection and the refinement statistics, the full characterization (^{1}H, ^{19}F, and ^{13}C NMR, IR, HRMS) of all the AR inhibitors and their key intermediates along with detailed working procedures for their preparation. This material is available free of charge via the Internet at http://pubs.acs.org.

■ AUTHOR INFORMATION

Corresponding Authors

*E-mail: fanfrlik@uochb.cas.cz.

*E-mail: podjarny@igbmc.fr.

Notes

The authors declare no competing financial interest.

■ ACKNOWLEDGMENTS

This work was part of the Research Project RVO: 61388963 of the Institute of Organic Chemistry and Biochemistry, Academy of Sciences of the Czech Republic. This work was also supported by the Czech Science Foundation [P208/12/G016], Gilead Sciences, Inc., the operational program Research and Development for Innovations of the European Social Fund (CZ 1.05/2.1.00/03/0058), the CNRS, the INSERM, the Université de Strasbourg, the Région Alsace, and the Hopital Civil de Strasbourg. The crystallographic experiments were performed on the X06SA beamline at the Swiss Light Source, Paul Scherrer Institut, Villigen, Switzerland. In particular, we thank T. Tomizaki and A. Pauluhn for their help on the beamline.

■ ABBREVIATIONS

SQM semiempirical quantum mechanical; AR aldose reductase; ARI aldose reductase inhibitor; P protein; L ligand; X-bond halogen bond; I inhibitor

■ REFERENCES

(1) Parisini, E., Metrangolo, P., Pilati, T., Resnati, G., and Terraneo, G. (2011) Halogen bonding in halocarbon−protein complexes: A structural survey. *Chem. Soc. Rev. 40*, 2267−2278.

(2) Auffinger, P., Hays, F. A., Westhof, E., and Ho, P. S. (2004) Halogen bonds in biological molecules. *Proc. Natl. Acad. Sci. U.S.A. 101*, 16789−16794.

(3) Lu, Y., Liu, Y., Xu, Z., Li, H., Liu, H., and Zhu, W. (2012) Halogen bonding for rational drug design and new drug discovery. *Expert Opin. Drug Discov. 7*, 375−383.

(4) Metrangolo, P., and Resnati, G. (2001) Halogen bonding: A paradigm in supramolecular chemistry. *Chem.—Eur. J. 7*, 2511−2519.

(5) Nguyen, L. H., Horton, P. N., Hursthouse, M. B., Legon, A. C., and Bruce, D. W. (2004) Halogen Bonding: A New Interaction for Liquid Crystal Formation. *J. Am. Chem. Soc. 126*, 16−17.

(6) Wilcken, R., Zimmermann, M. O., Lange, A., Joerger, A. C., and Boeckler, F. M. (2013) Principles and applications of halogen bonding in medicinal chemistry and chemical biology. *J. Med. Chem. 56*, 1363−1388.

(7) Kantsadi, A. L., Hayes, J. M., Manta, S., Skamnaki, V. T., Kiritsis, Ch., Psarra, A.-M. G., Koutsogiannis, Z., Dimopoulou, A., Theofanous, S., Nikoleousakos, N., Zoumpoulakis, P., Kontou, M., Papadopoulos, G., Zographos, S. E., Komiotis, D., and Leonidas, D. D. (2012) The σ-hole phenomenon of halogen atoms forms the structural basis of the strong inhibitory potency of C5 halogen substituted glucopyranosyl nucleosides towards glycogen phosphorylase b. *ChemMedChem. 7*, 722−732.

(8) Wilcken, R., Liu, X., Zimmermann, M. O., Rutherford, T. J., Fersht, A. R., Joerger, A. C., and Boeckler, F. M. (2012) Halogen-enriched fragment libraries as leads for drug rescue of mutant p53. *J. Am. Chem. Soc. 134*, 6810−6818.

(9) Fedorov, O., Huber, K., Eisenreich, A., Filippakopoulos, P., King, O., Bullock, A. N., Szklarczyk, D., Jensen, L. J., Fabbro, D., Trappe, J., Rauch, U., Bracher, F., and Knapp, S. (2011) Specific CLK inhibitors from a novel chemotype for regulation of alternative splicing. *Chem. Biol. 18*, 67−76.

(10) Hardegger, L. A., Kuhn, B., Spinnler, B., Anselm, L., Ecabert, R., Stihle, M., Gsell, B., Thoma, R., Diez, J., Benz, J., Plancher, J. M., Hartmann, G., Isshiki, Y., Morikam,i, K., Shimma, N., Haap, W., Banner, D. W., and Diederich, F. (2011) Halogen bonding at the active sites of human cathepsin L and MEK1 kinase: Efficient interactions in different environments. *ChemMedChem. 54*, 2048−2054.

(11) Baumli, S., Endicott, J. A., and Johnson, L. N (2010) Halogen bonds form the basis for selective P-TEFb inhibition by DRB. *Chem. Biol. 17*, 931−936.

(12) Xu, Z., Liu, Z., Chen, T., Chen, T., Wang, Z., Tian, G., Shi, J., Wang, X., Lu, Y., Yan, X., Wang, G., Jiang, H., Chen, K., Wang, S., Xu, Y., Shen, J., and Zhu, W. (2011) Utilization of halogen bond in lead optimization: a case study of rational design of potent phosphodiesterase type 5 (PDE5) inhibitors. *J. Med. Chem. 54*, 5607−5611.

(13) Lommerse, J. P. M., Stone, A. J., Taylor, R., and Allen, F. H. (1996) The nature and geometry of intermolecular interactions between halogens and oxygen or nitrogen. *J. Am. Chem. Soc. 118*, 3108−3116.

(14) Metrangolo, P., Neukirch, H., Pilati, T., and Resnati, G. (2005) Halogen bonding based recognition processes: A world parallel to hydrogen bonding. *Acc. Chem. Res. 38*, 386−395.

(15) Romaniello, P., and Lelj, F. (2002) Halogen bond in $(CH_3)(n)X$ (X = N, P, n = 3; X = S, n = 2) and $(CH_3)(n)XO$ (X = N, P, n = 3; X = S, n = 2) adducts with CF_3I. Structural and energy analysis including relativistic zero-order regular approximation approach in a density functional theory framework. *J. Phys. Chem. A 106*, 9114−9119.

(16) Politzer, P., Murray, J. S., and Clark, T. (2010) Halogen bonding: An electrostatically-driven highly directional noncovalent interaction. *Phys. Chem. Chem. Phys. 12*, 7748−7757.

(17) Politzer, P., Lane, P., Concha, M. C., Ma, Y., and Murray, J. S. (2007) An overview of halogen bonding. *J. Mol. Model. 13*, 305−311.

(18) Clark, T., Hennemann, M., Murray, J. S., and Politzer, P. (2007) Halogen bonding: The σ-hole. *J. Mol. Model. 13*, 291−296.

(19) Riley, K. E., Murray, J. S., Fanfrlík, J., Řezáč, J., Solá, R. J., Concha, M. C., Ramos, F. M., and Politzer, P. (2012) Halogen bond tunability II: The varying roles of electrostatic and dispersion contributions to attraction in halogen bonds. *J. Mol. Model.*, DOI: 10.1007/s00894-012-1428-x.

(20) Riley, K. E., Murray, J. S., Fanfrlík, J., Řezáč, J., Solá, R. J., Concha, M. C., Ramos, F. M., and Politzer, P. (2011) Halogen bond tunability I: The effects of aromatic fluorine substitution on the strengths of halogen-bonding interactions involving chlorine, bromine, and iodine. *J. Mol. Model. 17*, 3309−3318.

(21) Valerio, G., Raos, G., Meille, S. V., Metrangolo, P., and Rensati, G. (2000) Halogen bonding in fluoroalkylhalides: A quantum chemical study of increasing fluorine substitution. *J. Phys. Chem. A 104*, 1617−1620.

(22) Hardegger, L. A., Kuhn, B., Spinnler, B., Anselm, L., Ecabert, R., Stihle, M., Gsell, B., Thoma, R., Diez, J., Benz, J., Plancher, J. M., Hartmann, G., Banner, D. W., Haap, W., and Diederich, F. (2011) Systematic investigation of halogen bonding in protein−ligand interactions. *Angew. Chem., Int. Ed. 50*, 314−318.

(23) Petrash, J. M. (2004) All in the family: Aldose reductase and closely related aldo-keto reductases. *Cell. Mol. Life Sci. 61*, 737−749.

(24) Evans, J. L., Goldfine, I. D., Maddux, B. A., and Grodsky, G. M. (2002) Oxidative stress and stress-activated signalling pathways: a unifying hypothesis of type 2 diabetes. *Endocrine Rev. 23*, 599−622.

(25) Ramana, K. V., and Srivastava, S. K. (2010) Aldose reductase: a novel therapeutic target for inflammatory pathologies. *Int. J. Biochem. Cell Biol. 42*, 17−20.
(26) Yadav, U. C., Mishra, R., Aguilera-Aguirre, L., Sur, S., Bolodgh, I., Ramana, K. V., and Srivatsava, S. K. (2013) Prevention of allergic rhinitis by aldose reductase inhibition in a murine model. *Infl. Allergy Drug Targets 12*, 178−186.
(27) Tammali, R., Reddy, A. B., Saxena, A., Rychahou, P. G., Evers, B. M., Qiu, S., Awasthi, S., Ramana, K. V., and Srivastava, S. K. (2011) Inhibition of aldose reductase prevents colon cancer metastasis. *Carcinogenesis 32*, 1259−1267.
(28) Zeindl-Eberhart, E., Haraida, S., Liebmann, S., Jungblut, P. R., Lamer, S., Mayer, D., Jager, G., Chung, S., and Rabes, H. M. (2004) Detection and identification of tumor-associated protein variants in human hepatocellular carcinomas. *Hepatology 39*, 540−549.
(29) Ruiz, F., Hazemann, I., Mitschler, A., Joachimiak, A., Schneider, T., Karplus, M., and Podjarny, A. (2004) The crystallographic structure of the aldose reductase-IDD 552 complex shows direct proton donation from tyrosine, 48. *Acta Crystallogr., Sect. D 60*, 1347−1354.
(30) Howard, E. I., Sanishvili, R., Cachau, R. E., Mitschler, A., Chevrier, B., Barth, P., Lamour, V., Van Zandt, M., Sibley, E., Bon, C., Moras, D., Schneider, T. R., Joachimiak, A., and Podjarny, A. (2004) Ultrahigh resolution drug design I: Details of interactions in human aldose reductase−inhibitor complex at 0.66 A. *Proteins 55*, 792−804.
(31) Blakeley, M. P., Ruiz, F., Cachau, R., Hazemann, I., Meilleur, F., Mitschler, A., Ginell, S., Afonine, P., Ventura, O. N., Cousido-Siah, A., Haertlein, M., Joachimiak, A., Myles, D., and Podjarny, A. (2008) Quantum model of catalysis based on a mobile proton revealed by subatomic X-ray and neutron diffraction studies of h-aldose reductase. *Proc. Natl. Acad. Sci. U.S.A. 105*, 1844−1848.
(32) Fourier, B., Bendeif, E.-E., Guillot, B., Podjarny, A., Lecomte, C., and Jelsch, Ch. (2009) Charge density and electrostatic interactions of fidarestat, an inhibitor of human aldose reductase. *J. Am. Chem. Soc. 131*, 10929−10941.
(33) Steuber, H., Heine, A., and Klebe, G. (2007) Structural and thermodynamic study on aldose reductase: Nitro-substituted inhibitors with strong enthalpic binding contribution. *J. Mol. Biol. 368*, 618−638.
(34) Steuber, H., Czodrowski, P., Sotriffer, C. A., and Klebe, G. (2007) Tracing changes in protonation: A prerequisite to factorize thermodynamic data of inhibitor binding to aldose reductase. *J. Mol. Biol. 373*, 1305−1320.
(35) Koch, C., Heine, A., and Klebe, G. (2011) Tracing the detail: How mutations affect binding modes and thermodynamic signatures of closely related aldose reductase inhibitors. *J. Mol. Biol. 406*, 700−712.
(36) Koch, C., Heine, A., and Klebe, G. (2011) Ligand-induced fit affects binding modes and provokes changes in crystal packing of aldose reductase. *Biochem. Biochphys. Acta 1810*, 879−887.
(37) Podjarny, A., Cachau, R. E., Schneider, T., Van Zandt, M., and Joachimiak, A. (2004) Subatomic and atomic crystallographic studies of aldose reductase: Implications for inhibitor binding. *Cell. Mol. Life Sci. 61*, 763−773.
(38) Jurecka, P., Cerny, J., Hobza, P., and Salahub, D. (2007) Density functional theory augmented with an empirical dispersion term. Interaction energies and geometries of 80 noncovalent complexes compared with *ab initio* quantum mechanics calculations. *J. Comput. Chem. 28*, 555−569.
(39) Stewart, J. J. P. (2007) Optimization of parameters for semiempirical methods V: Modification of NDDO approximations and application to 70 elements. *J. Mol. Model. 13*, 1173−1213.
(40) Rezac, J., Fanfrlik, J., Salahub, D., and Hobza, P. (2009) Semiempirical quantum chemical PM6 method augmented by dispersion and H-bonding correction terms reliably describes various types of noncovalent complexes. *J. Chem. Theory Comput. 5*, 1749−1760.
(41) Rezac, J., and Hobza, P. (2012) Advanced corrections of hydrogen bonding and dispersion for semiempirical quantum mechanical methods. *J. Chem. Theory Comput. 8*, 141−151.
(42) Rezac, J., and Hobza, P. (2011) A halogen-bonding correction for the semiempirical PM6 method. *Chem. Phys. Lett. 506*, 286−289.
(43) Wang, J., Wolf, R. M., Caldwell, J. W., Kollman, P. A., and Case, D. A. (2004) Development and testing of a general AMBER Force Field. *J. Comput. Chem. 25*, 1157−1174.
(44) Bayly, C. I., Cieplak, P., Cornell, W., and Kollman, P. A. (1993) Well-behaved electrostatic potential based method using charge restraints for determining atom-centered charges: The RESP model. *J. Phys. Chem. 97*, 10269−10280.
(45) Fanfrlik, J., Bronowska, A. K., Rezac, J., Prenosil, O., Konvalinka, J., and Hobza, P. (2010) A reliable docking/scoring scheme based on the semiempirical quantum mechanical PM6-DH2 method accurately covering dispersion and H-bonding: HIV-1 protease with 22 ligands. *J. Phys. Chem. B. 114*, 12666−12678.
(46) Lepšík, M., Řezáč, J., Kolář, M., Pecina, A., Hobza, P., and Fanfrlík, J. (2013) The semiempirical quantum mechanical scoring function for *in silico* drug design. *ChemPlusChem 78*, 921−931.
(47) Dobeš, P., Fanfrlík, J., Řezáč, J., Otyepka, M., and Hobza, P. (2011) Transferable scoring function based on semiempirical quantum mechanical PM6-DH2 method: CDK2 with 15 structurally diverse inhibitors. *J. Comput.-Aided Mol. Des. 25*, 223−235.
(48) Brahmkshatriya, P. S., Dobeš, P., Fanfrlík, J., Řezáč, J., Paruch, K., Bronowska, A. K., Lepšík, M., and Hobza, P. (2013) Quantum mechanical scoring: Structural and energetic insights into cyclin-dependent kinase 2 inhibition by pyrazolo[1,5-a]pyrimidines. *Curr. Comput.-Aided Drug Des. 9*, 118−129.
(49) Dobeš, P., Řezáč, J., Fanfrlík, J., Otyepka, M., and Hobza, P. (2011) Semiempirical quantum mechanical method PM6-DH2X describes the geometry and energetics of CK2−inhibitor complexes involving halogen bonds well, while the empirical potential fails. *J. Phys. Chem. B 115*, 8581−8589.
(50) Van Zandt, M., Jones, M., Gunn, D., Geraci, L., Jones, J., Sawicki, D., Sredy, J., Jacot, J., Dicioccio, A., Petrova, T., Mitschler, A., and Podjarny, A. (2005) Discovery of 3-[(4,5,7-trifluorobenzothiazol-2-yl)methyl]indole-N-acetic acid (lidorestat) and congeners as highly potent and selective inhibitors of aldose reductase for treatment of chronic diabetic complications. *J. Med. Chem. 48*, 3141−3152.
(51) Barski, O. A., Tipparaju, S. M., and Bhatnagar, A. (2008) The aldo-keto reductase superfamily and its role in drug metabolism and detoxification. *Drug Metab. Rev. 40*, 553−624.
(52) Case, D. A., Darden, T. A., Cheatham, III, T. E., Simmerling, C. L., Wang, J., Duke, R. E., Luo, R., Crowley, M., Walker, R. C., Zhang, W., Merz, K. M., Wang, B., Hayik, S., Roitberg, A., Seabra, G., Kolossvary, I., Wong, K. F., Paesani, F., Vanicek, J., Wu, X., Brozell, S. R., Steinbrecher, T., Gohlke, H., Yang, L., Tan, C., Mongan, J., Hornak, V., Cui, G., Mathews, D. H., Seetin, M. G., Sagui, C., Babin, V., and Kollman, P. A. AMBER 10, University of California, San Francisco, 2008.
(53) Marenich, A. V., Cramer, C. J., and Truhlar, D. G. (2009) Universal solvation model based on solute electron density and on a continuum model of the solvent defined by the bulk dielectric constant and atomic surface tensions. *J. Phys. Chem. B 113*, 6378−6396.
(54) Frisch, M. J., Trucks, G. W., Schlegel, H. B., Scuseria, G. E., Robb, M. A., Cheeseman, J. R., Scalmani, G., Barone, V., Mennucci, B., Petersson, G. A., Nakatsuji, H., Caricato, M., Li, X., Hratchian, H. P., Izmaylov, A. F., Bloino, J., Zheng, G., Sonnenberg, J. L., Hada, M., Ehara, M., Toyota, K., Fukuda, R., Hasegawa, J., Ishida, M., Nakajima, T., Honda, Y., Kitao, O., Nakai, H., Vreven, T., Montgomery, Jr., J. A., Peralta, J. E., Ogliaro, F., Bearpark, M., Heyd, J. J., Brothers, E., Kudin, K. N., Staroverov, V. N., Kobayashi, R., Normand, J., Raghavachari, K., Rendell, A., Burant, J. C., Iyengar, S. S., Tomasi, J., Cossi, M., Rega, N., Millam, N. J., Klene, M., Knox, J. E., Cross, J. B., Bakken, V., Adamo, C., Jaramillo, J., Gomperts, R., Stratmann, R. E., Yazyev, O., Austin, A. J., Cammi, R., Pomelli, C., Ochterski, J. W., Martin, R. L., Morokuma, K., Zakrzewski, V. G., Voth, G. A., Salvador, P., Dannenberg, J. J., Dapprich, S., Daniels, A. D., Farkas, Ö., Foresman, J. B., Ortiz, J. V., Cioslowski, J., and Fox, D. J. (2009) *Gaussian09*, Gaussian, Inc., Wallingford, CT.

(55) Kolář, M., Fanfrlík, J., Lepšík, M., Forti, F., Luque, F. J., and Hobza, P. (2013) Assessing the accuracy and performance of implicit solvent models for drug molecules: Conformational ensemble approaches. *J. Phys. Chem. B 117*, 5950−5962.
(56) Kolář, M., and Hobza, P. (2012) On extension of current biomolecular force field for the description of halogen bonds. *J. Chem. Theory Comput. 8*, 1325−1333.
(57) Klamt, A. (1995) Conductor-like solvent model for real solvents: A new approach to the quantitative calculation of solvation phenomena. *J. Phys. Chem. 99*, 2224−2235.
(58) Kolář, M., Hobza, P., and Bronowska, A. K. (2013) Plugging the explicit σ-holes in molecular docking. *Chem. Commun. 49*, 981−983.
(59) Dapprich, S., Komaromi, I., Suzie Byun, K., Morokuma, K., and Frisch, M. J. (1999) A new ONIOM implementation in Gaussian98. Part I. The calculation of energies, gradients, vibrational frequencies, and electric field derivatives. *J. Mol. Struct. Theochem. 461−462*, 1−21.
(60) J. Řezáč, *Cuby3*, Prague.
(61) Ahlrichs, R., Bar, M., Haser, M., Horn, H., and Kolmel, C. (1989) Electronic structure calculations on workstation computers: The program system Turbomole. *Chem. Phys. Lett. 162*, 165−169.
(62) Stewart, J. J. P. (2009) *MOPAC2009*, Stewart Computational Chemistry, Colorado Springs, CO; http://OpenMOPAC.net.
(63) Walker, R. C., de Souza, M. M., Mercer, I. P., Gould, I. R., and Klug, D. R. (2002) Large and fast relaxations inside a protein: Calculation and measurement of reorganization energies in alcohol dehydrogenase. *J. Phys. Chem. B 106*, 11658−11665.
(64) Holmberg, N., Ryde, U., and Bülow, L. (1999) Redesign of the coenzyme specificity in L-lactate dehydrogenase from *Bacillus stearothermophilus* using site-directed mutagenesis and media engineering. *Protein Eng. 12*, 851−856.
(65) Pavelites, J. J., Gao, J. L., Bash, P. A., and Mackerell, A. D. (1997) A molecular mechanics force field for NAD+, NADH, and the pyrophosphate groups of nucleotides. *J. Comput. Chem. 18*, 221−239.
(66) Bitzek, E., Koskinen, P., Gahler, F., Moseler, M., and Gumbsch, P. (2006) Structural relaxation made simple. *Phys. Rev. Lett. 97*, 170201−170205.
(67) Pearlman, D. A., and Charifson, P. S. (2001) Are free energy calculations useful in practice? A comparison with rapid scoring functions for the p38 MAP kinase protein system. *J. Med. Chem. 44*, 3417−3423.
(68) Winn, M. D., Ballard, C. C., Cowtan, K. D., Dodson, E. J., Emsley, P., Evans, P. R., Keegan, R. M., Krissinel, E. B., Leslie, A. G., McCoy, A., McNicholas, S. J., Murshudov, G. N., Pannu, N. S., Potterton, E. A., Powell, H. R., Read, R. J., Vagin, A., and Wilson, K. S. (2011) Overview of the CCP4 suite and current developments. *Acta Crystallogr., Sect. D: Biol. Crystallogr. 67*, 235−242.
(69) Adams, P. D., Afonine, P. V., Bunkoczi, G., Chen, V. B., Davis, I. W., Echols, N., Headd, J. J., Hung, L. W., Kapral, G. J., Grosse-Kunstleve, R. W., McCoy, A. J., Moriarty, N. W., Oeffner, R., Read, R. J., Richardson, D. C., Richardson, J. S., Terwilliger, T. C., and Zwart, P. H. (2010) PHENIX: A comprehensive Python-based system for macromolecular structure solution. *Acta Crystallogr., Sect. D; Biol. Crystallogr. 66*, 213−221.
(70) Emsley, P., Lohkamp, B., Scott, W. G., and Cowtan, K. (2010) Features and development of Coot. *Acta Crystallogr., Sect. D; Biol. Crystallogr. 66*, 486−501.